Magnetic cylindrical nanowires with single modulated diameter

S. Allende
Departamento de Física, FCFM, Universidad de Chile, Casilla 487-3, Santiago, Chile;
Departamento de Física, Universidad de Santiago de Chile (USACH), Av. Ecuador 3493, Santiago, Chile;
and Center for the Development of Nanoscience and Nanotechnology, 9170124, Estación Central, Santiago, Chile

D. Altbir
Departamento de Física, Universidad de Santiago de Chile (USACH), Av. Ecuador 3493, Santiago, Chile
and Center for the Development of Nanoscience and Nanotechnology, 9170124, Estación Central, Santiago, Chile

K. Nielsch
Institute of Applied Physics, University of Hamburg, Jungiusstrasse 11, 20355 Hamburg, Germany
(Received 26 February 2009; revised manuscript received 29 July 2009; published 9 November 2009)

Nucleation and propagation of a domain wall along a modulated wire as a function of its geometry has been investigated. In all the cases, nucleation began at the thicker section and propagated toward the thinner section, regardless of the reversal mode. At the interface, the wall was pinned and a higher nucleation field was required to continue the propagation of the wall. This behavior led to the existence of two nucleation fields along each branch of the hysteresis curve.

DOI: 10.1103/PhysRevB.80.174402 PACS number(s): 75.75.+a

I. INTRODUCTION

In recent years, particles with sizes on the order of nanometers have attracted much attention because of experimental progress in their synthesis, which has led to an extraordinary control of their dimensions, as well as their potential for technological applications.[1,2] Among the different geometries considered, nanowires have been the focus of intense investigation. Fabrication techniques produce hexagonal arrays of Ni nanowires with long-range order and well-controlled geometry.[3] These particles have been proposed as high-resolution magnetic field sensors and nonvolatile magnetic memory devices. The reversal of the magnetization in these wires occurs by means of the nucleation and propagation of a domain wall. The precise understanding and control of both processes is fundamental for applications.

The most common technique used to fabricate nanowire arrays is the deposition of material on a template of nanoporous anodic aluminum oxide with self-organized hexagonal arrays of uniformly parallel nanopores. In this case, the diameter of the nanopores is constant, resulting in nanowires with a fixed diameter along their axis. Lee *et al.*[4,5] recently obtained a different template by combining two different processes hard anodization and mild anodization, in which the diameter of the pore can be modulated [see Fig. 3(d) of Ref. 5]. Single modulated nanowires, which are the focus of this paper, can be fabricated by a simpler approach. First, Al_2O_3 pore structures are grown to a certain depth and the pore diameter is enhanced by chemical etching. Subsequently, the growth of the pore is continued with the initial pore diameter. Alternatively, macroporous silicon is an ideal template system for the growth of modulated pores[6] and the production of gold nanowires with modulated pore diameter.[7]These templates open the way for production of arrays of nanowires with modulated diameter that can exhibit new and interesting properties.

In this work, we studied the magnetization reversal of nanowires with modulated diameter. We focused on the nucleation of the domain wall, which drives the reversal of the magnetization.

II. MODEL

Our starting point was a uniform Ni nanowire with modulated diameter d and length ℓ, as illustrated in Fig. 1. The wire was formed by three sections. At the ends, it had sections with diameters d_1 and d_2, with $d_2 > d_1$, and lengths l_1 and l_2. The interface between both sections had a length $w_d = 100$ nm and a variable diameter d, which we modeled as $d(z) = (d_1 - d_2)(z - l_1)/100 + d_1$, where $z=0$ corresponds to the thinner end. This expression is valid only at the interface.

The internal energy E of a nanowire with modulated diameter with N magnetic moments can be written as $E = \Sigma_{j>i}^{N} E_{ij}^{d} - J\Sigma_{ij\in\{nn\}} \hat{\mu}_i \cdot \hat{\mu}_j + \Sigma_{i=1}^{N} E_i^a$, where E_{ij}^d is the dipolar energy given by $E_{ij}^d = [\vec{\mu}_i \cdot \vec{\mu}_j - 3(\vec{\mu}_i \cdot \hat{n}_{ij})(\vec{\mu}_j \cdot \hat{n}_{ij})]/r_{ij}^3$, with r_{ij} being the distance between the magnetic moments $\vec{\mu}_i$ and $\vec{\mu}_j$, $\hat{\mu}_i$ is the unit vector along the direction of $\vec{\mu}_i$, and $\hat{n}_{ij}$ is the unit vector along the direction that connects $\vec{\mu}_i$ and $\vec{\mu}_j$. J is the exchange coupling constant between nearest neighbors and the Zeeman contribution $E_i^a = -\vec{\mu}_i \cdot \vec{H}_a$. In this work, we

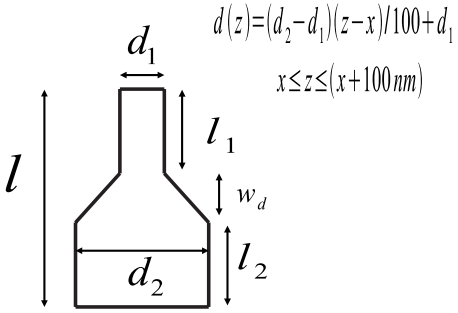

FIG. 1. Geometrical parameters of a nanowire with modulated diameter.

investigated Ni nanowires built along the [100] direction of a fcc lattice with lattice parameter $a_0=3.52$ Å. We used $\mu_i=0.61\mu_B$ and $J=3.5$ meV. We focused on nanowires with diameters varying from 30 to 120 nm and lengths of 1.1 and 1.3 μm.The wires always have an aspect ratio greater than 10 and their surface-to-volume ratio is less than 0.1. In our case, the highest ratio obtained between the anisotropic surface energy and the magnetostatic energy was 0.001 for a wire with radius=15 nm and length=1300 nm, where all the magnetic moments are along the axis of the wire, and the magnetic anisotropy constant value for Ni is on the order of 0.1 erg/cm^2.[8] The last result means that the most important anisotropy is the shape anisotropy, which comes from the internal magnetostatic energy, so surface effects are not significant. Such wires contain about 10^8 atoms, which is beyond the scope of a regular Monte Carlo (MC) simulation, including dipolar interactions, considering the available computational resources. In order to reduce the number of interacting atoms, we made use of a scaling technique proposed by d'Albuquerque *et al.*,[9] originally formulated to investigate the equilibrium phase diagram of cylindrical particles of height h and diameter d. The authors showed that this diagram is equivalent to that for a smaller particle with $d'=d\chi^\eta$ and $h'=h\chi^\eta$, with $\chi<1$ and $\eta\approx0.56$, if the exchange constant is also scaled as $J'=\chi J$. We used this idea starting from the desired value for the total number of interacting particles N that we could deal with based on the computational facilities currently available and estimated N of the order of 10^3. With this in mind, we obtained the scale value $\chi=8\times10^{-4}$. It has also been shown that the scaling relations can be used together with MC simulations and result in good agreement with experiments and micromagnetic calculations.[10–13]

MC simulations were carried out at $T=300$ K, using the Metropolis algorithm,[14] in which the new orientation of the magnetic moments is restricted according to Nowak *et al.*[15] It is important to mention that Monte Carlo simulations consider essentially the energy of the system. Effects related to magnetization dynamics, such as torque and magnetization precession, have not been considered in our calculations. We started our simulations at $H_a=2$ kOe, which is higher than the saturation field, with all the magnetic moments of the wire parallel to $\vec{H}_a$. The field was then linearly decreased at a rate of $\Delta H=0.01$ kOe for every 300 MC steps. In this way, about 120 000 MC steps are needed to go from saturation to the coercive field.

III. RESULTS

We fixed $w_d=0.1$ μm and $L=1.1$ μm for our first series of calculations. We started simulating a wire with $d_1=65$ nm and $d_2=130$ nm. If the entire wire had any of both diameters, the magnetization reversal occurred by means of the nucleation and propagation of a vortex wall. The hysteresis curves (with normalized magnetization) corresponding to a fixed diameter of 65 and 130 nm are illustrated with a dotted-dashed (red online) and dotted (black online) curves, respectively. The hysteresis curves of modulated wires with $l_1=800$ and 500 nm are depicted with a solid (green online) and a dashed curve (blue online) in Fig. 2, where it is seen that when both sections have the same length, the reversal is fully dominated by the thick section, which, due to the different diameters, has the greatest magnetic volume. In this case, the nucleation field of the modulated wire almost coincides with that of the uniform wire with a diameter of 130 nm.

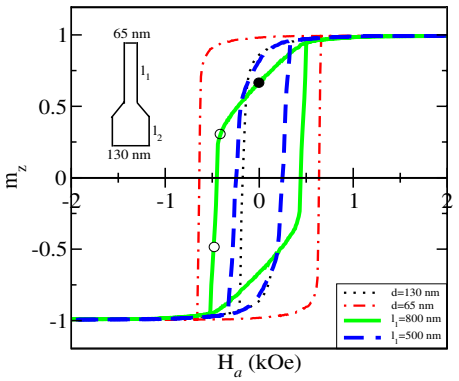

FIG. 2. (Color online) Hysteresis curves for modulated wires with $d_1=65$ nm, $d_2=130$ nm, and $l_1=500$ nm, 800 nm. $l=1.1$ μm. The dots represent three different times whose magnetization profiles are illustrated in Fig. 3

We also investigated a wire, in which the magnetic volumes of both uniform sections are equal. That occurs for $l_1=800$ nm and $l_2=200$ nm. In this case, the hysteresis exhibits a complex behavior. The coercivity, as expected, shows a value intermediate between the values of the uniform wires. However, the remanence is lower. Two different nucleation fields appear related to the reversal at each section $H_{N1}=1.0$ kOe and $H_{N2}=-0.43$ kOe. To understand this behavior, we monitored the reversal by the values of $\mu_i=m_i/m$, $i=x$, y, and z, which are the average values of the magnetic-moment components relative to the saturation value. The solid line represents the average axial component of the magnetization m_z, while the other two in-plane components are given by the dotted and dashed lines. When m_x and m_y both average to zero, we face a vortex. If one or both of these components are nonzero, it is a transverse wall that is observed. The upper image represents the magnetization profile at a moment depicted by a black dot in Fig. 3. In this particular case, the reversal begins at the end of the thicker wire, with the magnetization forming a vortex. Subsequently, a second vortex with opposite chirality forms in the thicker wire near the interface. While decreasing the field, the reversal continues, reaching the thinner wire, as illustrated in the middle image. In this region, magnetization reversal is very fast and is driven by the propagation of a vortex domain wall. The position of the wall is determined by the maximum of $1-|m_z|$ and is clearly seen in the lower image in Fig. 3(c) at $L=633$ nm.

In order to observe a transverse reversal mode, we modeled a wire with $d_1=32.5$ nm and $d_2=65$ nm for $l_1=500$ and 800 nm (see Fig. 4). Our results for a uniform wire with a diameter of 65 nm are depicted by a dotted line (black online), while the dashed-dotted line (red online) represents the hysteresis of a uniform wire with 32.5 nm diameter, in which

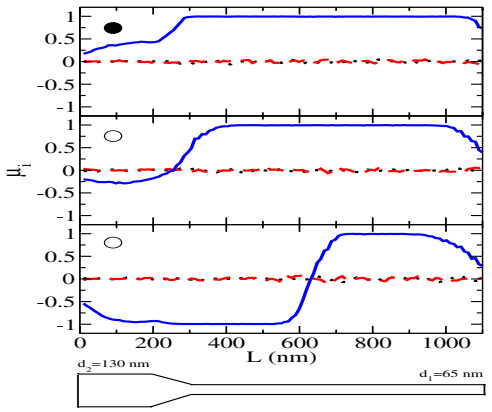

FIG. 3. (Color online) Magnetization profile for $d_1=65$ nm, $d_2=130$ nm, $l_1=800$ nm, $l_2=200$ nm, and $l=1.1$ nm. The curves represent $\mu_i=m_i/m$, $i=x$ (dashed line), y (dotted line), and z (solid line), which are the average values of the magnetic-moment components relative to their saturation value.

the magnetization reversal occurs via the propagation of a transverse wall (see Fig. 5). These results are in agreement with previous results on cylindrical[16] and planar nanowires.[17] In the modulated wire, when $l_1=500$ nm, the reversal starts at the free end of the thicker wire with the nucleation of a vortex. Another vortex with opposite chirality rapidly nucleates at the thicker interface. After the reversal of all the thicker section, the reversal continues into the thinner section with a transverse domain wall. Both remanence and coercivity are very similar to the values observed for a uniform wire of 65 nm diameter. The hysteresis of this modulated wire is depicted by a dashed line (blue online) in Fig. 4.

When $l_1=800$ nm, the reversal again starts with a vortex at the thicker wire, and when it propagates through the thinner wire, the vortex is lost and a transverse wall appears. In this case, the coercivity is slightly lower than that of a uniform wire of 65 nm diameter. The values of the coercivity show the strong influence of the section of higher magnetic volume. This behavior is illustrated by the images in Fig. 5.

We now investigate the effect of varying d_1 for constant $d_2=120$ nm, $l_1=1000$ nm, $l_2=200$ nm, and $w_d=100$ nm. The hystereses for $d_1=30$, 45, and 60 nm are depicted in Fig.

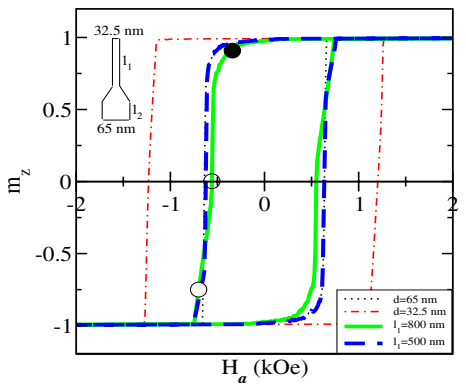

FIG. 4. (Color online) Hysteresis curves for modulated wires with $d_1=32.5$ nm, $d_2=65$ nm, and $l_1=500$ nm, 800 nm. $l=1.1$ μm.

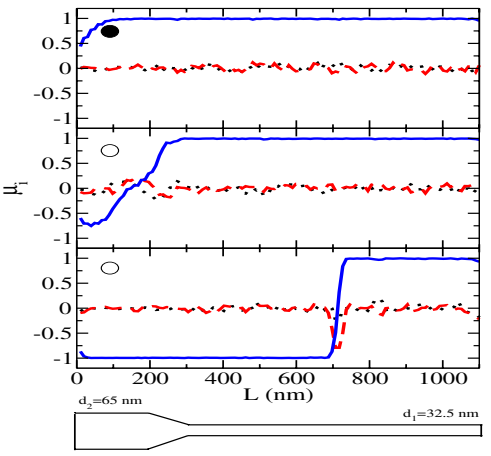

FIG. 5. (Color online) Magnetization profile for $d_1=32.5$ nm, $d_2=65$ nm, $l_1=800$ nm, $l_2=200$ nm, and $l=1.1$ nm. The curves represent $\mu_i=m_i/m$, $i=x$ (dashed line), y (doted line), and z (solid line), which are the average values of the magnetic-moment components relative to its saturation value.

6. In these cases, the same as in Fig. 2 for $l_1=l_2$, two different nucleation fields appear related to the reversal of each section. If we examine the wire with of $d_1=45$ nm, the first nucleation field for this diameter is $H_{N1}=0.6$ kOe and the second nucleation field is $H_{N2}=-0.39$ kOe. The reversal in these three wires starts, as expected, at the thicker end forming a vortex state. The reversal of the thinner wire, which starts at the higher nucleation field, is driven by a transverse wall.

In order to investigate the response of these wires in depth, we set the field at a value between both nucleation fields and let the wire relax under that field. Figure 7 shows snapshots of the magnetization of the wire with $d_2=45$ nm at two different times $t_1=60.000$ MCS and $t_2=120.000$ MCS at $H_a=-0.3$ kOe. By comparing both figures, we can conclude that the vortex state that appears in the thicker section is stable and that in order to continue the reversal along the thinner sections, a higher negative field is required.

Finally, we investigate a wire with $d_1=30$ nm, $d_2=45$ nm, $l_1=692$ nm, and $l_2=308$ nm. These lengths were

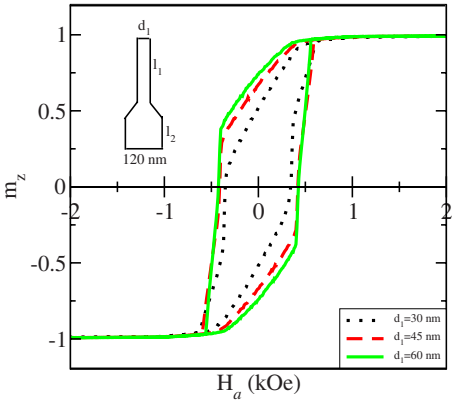

FIG. 6. (Color online) Hysteresis curves for modulated wires with $d_1=30$ nm, 45 nm, 60 nm, and $d_2=130$ nm. $l_1=1000$ nm, and $l_2=200$. $l=1.3$ μm.

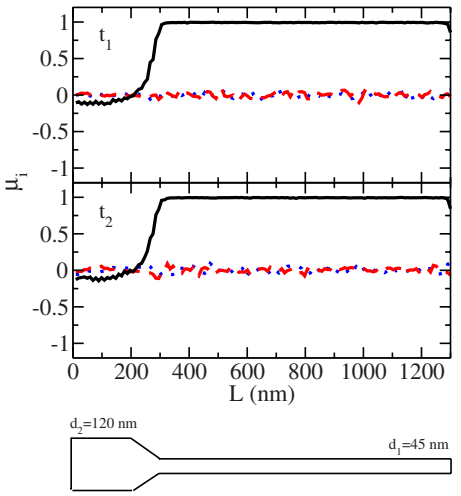

FIG. 7. (Color online) Magnetization profile for $d_1=45$ nm, $d_2=120$ nm, $l_1=1000$ nm, $l_2=200$ nm, and $l=1.3$ nm at $H_a=-0.3$ kOe. The curves represent $\mu_i=m_i/m$, $i=x$ (dashed line), y (doted line), and z (solid line), which are the average values of the magnetic-moment components relative to the saturation value.

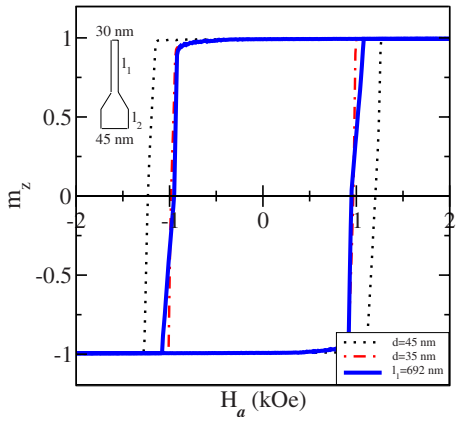

FIG. 8. (Color online) Hysteresis curves for modulated wires with $d_1=30$ nm, $d_2=45$ nm, and $l_2=308$ nm. $l=1.1$ μm.

chosen in order to have almost the same magnetic volume in each section. The hysteresis of this modulated wire is illustrated in Fig. 8 by a solid line (blue online), evidencing the existence of two nucleation fields $H_{N1}=-0.85$ kOe and $H_{N2}=-0.95$ kOe. The reversal is of transverse nature along both sections, starting at the thicker end.

IV. DISCUSSION AND CONCLUSIONS

In this paper, we have studied the nucleation and propagation of a domain wall along a modulated wire. In all the cases, nucleation starts at the thicker section and propagates toward the thinner section, regardless of the reversal mode. The reversal mode was determined by the geometry of each section. In Ni nanowires, for diameters below a limit of approximately 55 nm, inversion of the magnetization is driven by the nucleation and propagation of a transverse wall, while for diameters beyond the limit of 55 nm, the inversion starts with the nucleation of a vortex wall. The switching between the vortex and the transverse reversal mode when the radius decreases can be understood by looking at the competition between dipolar and exchange energies. The dipolar long-range energy decreases when the magnetic moments present a vortex state, and the short-range exchange term decreases by perfect alignment of the magnetic moments. Because the dipolar contribution is much smaller than the exchange term, it requires a high volume in order to form a vortex and decrease the total energy. Then, for large radius, the dipolar contribution favors the nucleation of a vortex wall. When the radius decreases, the exchange interaction between magnetic moments that are in the same cross section of the wire increases if they form a vortex. The large values of the magnetization gradient (exchange contribution) lead to particularly unfavorable energy. This phenomenon becomes particularly acute for wires with diameter on the order of a few times the exchange length (8 nm for Ni). In this case, the transverse mode becomes more favorable. This transition were previously reported and analyzed by Hertel[18] and Forster *et al.*[19] in wires and Landeros *et al.*[13] for tubes. Coercivity is dominated by the behavior of the section with the greater magnetic volume. At the interface, the wall is pinned and a higher nucleation field is required to continue the propagation of the wall. This behavior is in agreement with results previously reported by Wernsdorfer *et al.*[20] They investigated the magnetization switching in individual Ni nanowires and observed, in some samples, the pinning and depinning of a domain wall evidenced by the presence of several jumps in the hysteresis curves. This behavior was explained as the result of shape defects of the wire.

Nanowires with a planar geometry[21–27] have been investigated by other groups. Similar to our theoretical study, these investigations have focused on the pinning of domain walls in nanowires with tailored defect sides and the propagation of domain walls.[23,27] In contrast to planar nanowires, cylindrical nanowires exhibit significantly different physical properties. For example, the core of a vortex-type domain wall in cylindrical nanowires is always parallel to the axis, while in planar wires, due to the strong confinement in height, the vortex core points perpendicularly to the substrate plane. Furthermore, planar and cylindrical nanowires will exhibit variations, e.g., in the domain-wall velocity or the current-induced domain-wall propagation, which gives promising opportunities for further theoretical and experimental research on modulated nanowires.

ACKNOWLEDGMENTS

This work was supported by German Science Foundation DFB in the framework of the Sonderforschungsbereich Grant No. SFB 668 (Magnetismus vom Einzelatom zur Nanostruktur). In Chile we acknowledge the support from Millennium Science Nucleus "Basic and Applied Magnetism" (Project No. P06022F), Fondecyt (Grants No. 3090047 and No. 1080300), Financiamiento Basal para Centros Científicos y Tecnológicos de Excelencia, and AFOSR USA (Award No. FA9550-07-1-0040).

[1] S. Sun, C. B. Murray, D. Weller, L. Folks, and A. Moser, Science **287**, 1989 (2000).
[2] Th. Gerrits, H. A. M. van den Berg, J. Hohlfeld, L. Bar, and Th. Rasing, Nature (London) **418**, 509 (2002).
[3] K. Nielsch, R. B. Wehrspohn, J. Barhel, J. Kirschner, and U. Gösele, Appl. Phys. Lett. **79**, 1360 (2001).
[4] W. Lee, U. Gösele, and K. Nielsch, Nature Mater. **5**, 741 (2006).
[5] W. Lee, K. Schwirn, M. Steinhart, E. Pippel, R. Scholz, and U. Gösele, Nat. Nanotechnol. **3**, 234 (2008).
[6] S. Matthias, F. Müller, C. Jamois, R. B. Wehrspohn, and U. Gösele, Adv. Mater. **16**, 2166 (2004).
[7] S. Matthias, J. Schilling, K. Nielsch, F. Müller, R. B. Wehrspohn, and U. Gösele, Adv. Mater. **14**, 1618 (2002).
[8] H. Takayama, K.-P. Bohnen, and P. Fulde, Phys. Rev. B **14**, 2287 (1976).
[9] J. d'Albuquerque e Castro, D. Altbir, J. C. Retamal, and P. Vargas, Phys. Rev. Lett. **88**, 237202 (2002).
[10] P. Vargas, D. Altbir, and J. d'Albuquerque e Castro, Phys. Rev. B **73**, 092417 (2006).
[11] M. Bahiana, F. S. Amaral, S. Allende, and D. Altbir, Phys. Rev. B **74**, 174412 (2006).
[12] J. Mejia-Lopez, D. Altbir, A. H. Romero, X. Battle, I. V. Roshchin, C.-P. Li, and I. K. Schuller, J. Appl. Phys. **100**, 104319 (2006).
[13] P. Landeros, S. Allende, J. Escrig, E. Salcedo, D. Altbir, and E. E. Vogel, Appl. Phys. Lett. **90**, 102501 (2007).
[14] K. Binder and D. W. Heermann, *Monte Carlo Simulation in Statistical Physics* (Springer, New York, 2002).
[15] U. Nowak, R. W. Chantrell, and E. C. Kennedy, Phys. Rev. Lett. **84**, 163 (2000).
[16] R. Hertel and J. Kirschner, Physica B **343**, 206 (2004).
[17] O. Petracic, P. Szary, H. Zabel, D. Görlitz, and K. Nielsch, Superlattices and Microstruct. (to be published).
[18] R. Hertel, J. Magn. Magn. Mater. **249**, 251 (2002).
[19] H. Forster, T. Schreß, W. Scholz, D. Suess, V. Tsiantos, and J. Fidler, J. Magn. Magn. Mater. **249**, 181 (2002).
[20] W. Wernsdorfer, K. Hasselbach, A. Benoit, B. Barbara, B. Doudin, J. Meier, J.-Ph. Ansermet, and D. Mailly, Phys. Rev. B **55**, 11552 (1997).
[21] S. P. Parkin, M. Hayashi, and L. Thomas, Science **320**, 190 (2008).
[22] D. A. Allwood, Gang Xiong, M. D. Cooke, C. C. Faulkner, D. Atkinson, N. Vernier, and R. P. Cowburn, Science **296**, 2003 (2002).
[23] Y. Nakatani, A. Thiaville, and J. Miltat, J. Magn. Magn. Mater. **290-291**, 750 (2005).
[24] T. Shiratori, E. Fujii, Y. Miyaoka, and Y. Hozumi, J. Magn. Soc. Jpn. **22**, Supp. No. S2, 47 (1998).
[25] D. Atkinson, D. A. Allwood, Gang Xiong, M. D. Cooke, C. C. Faulkner, and R. P. Cowburn, Nature Mater. **2**, 85 (2003).
[26] M. Hayashi, L. Thomas, C. Rettner, R. Moriya, X. Jiang, and S. S. P. Parkin, Phys. Rev. Lett. **97**, 207205 (2006).
[27] Y. Nakatani, A. Thiaville, and J. Miltat, Nature Mater. **2**, 521 (2003).